

Critical Analysis of the Crystal Orientation Behavior in Polyethylene-Based Crystalline–Amorphous Diblock Copolymer

Ming-Champ Lin,[†] Yi-Chin Wang,[†] Hsin-Lung Chen,^{*,†} Alejandro J. Müller,[‡] Chun-Jen Su,[§] and U-Ser Jeng[§]

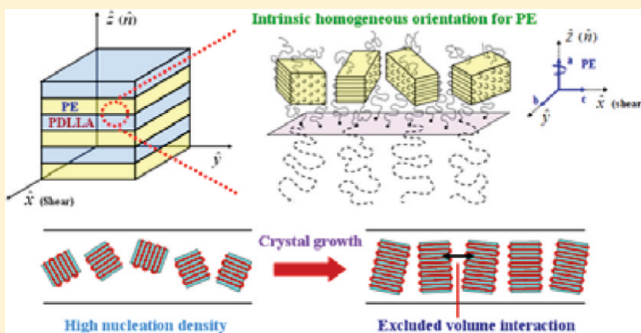
[†]Department of Chemical Engineering, National Tsing Hua University, Hsin-Chu 30013, Taiwan

[‡]Departamento de Ciencia de los Materiales, Grupo de Polímeros USB, Apartado 89000-A, Caracas, Venezuela

[§]National Synchrotron Radiation Research Center, Hsin-Chu 300, Taiwan

Supporting Information

ABSTRACT: Orientation of polyethylene (PE) crystals formed over a broad range of undercooling in a polyethylene-*b*-poly(D,L-lactide) (PE-*b*-PDLLA) diblock copolymer has been critically examined. Due to the large segregation strength and approximate 50/50 composition in this system, the crystallization took place within one-dimensionally confined lamellar micro-domains without forming spherulites. A homogeneous crystal orientation with the PE crystalline stems orienting parallel to the lamellar interface was observed at crystallization temperatures (T_c) between 45 and 102 °C. Once the sample was crystallized at $T_c \leq 40$ °C or directly quenched into liquid nitrogen from the melt, the isotropic WAXD pattern indicated that the PE crystals became randomly oriented. Considering that homeotropic orientation was not identified for the present system and other PE-based crystalline–amorphous diblocks, we concluded that PE crystals in the lamellar microdomains always show homogeneous orientation when there is a preferred orientational order. We further organized the thermodynamic and kinetic factors that may govern the preferred crystal orientation in diblock copolymers and concluded that the orientational order should be controlled by the competition between nucleation and crystal growth kinetics. The persistence of homogeneous orientation of PE was attributed to its excellent nucleating power.



INTRODUCTION

Incorporation of crystallization into the self-organization mechanism of block copolymers is an effective route to enrich their morphology and property.^{1–15} It has been established that the morphology formed after crystallization in diblock copolymer composed of a crystalline (C) and an amorphous (A) block is determined by the interplay among the segregation strength in the melt, the crystallization driving force of the C block, and the vitrification of the A block. When the glass transition temperature of the A block (T_g^A) is higher than the crystallization temperature (T_c), the crystallization can be effectively restricted within the microdomains surrounded by the hard glassy matrix established by the microphase separation.^{16–21} If T_g^A is lower than T_c , the amorphous block may provide a soft-confinement environment for the crystallization of the C block once the segregation strength is sufficiently strong.^{10,19,21–24}

In the case where the crystallization is confined within the microdomains, it has been recognized that the crystals formed may display preferred orientation with respect to the domain interface. Early studies of several poly(ethylene oxide) (PEO)-containing diblocks have revealed a “homeotropic” crystal orientation, where the direction of the crystalline stem (i.e., the *c*-axis) is aligned parallel to the normal (\hat{n}) of the lamellar domain interface.^{25–28} However, recent systematic studies of poly(ethylene oxide)-*b*-polystyrene (PEO-*b*-PS) by Zhu et al. found that

PEO crystal orientation indeed depended on crystallization temperature.¹⁴ When the diblock was quickly quenched into liquid nitrogen, the PEO crystals were randomly oriented within the lamellar microdomains. The crystals started to show preferred orientation when T_c was higher than –50 °C. The orientation of the *c*-axis with respect to the lamellar normal transformed from perpendicular (i.e., homogeneous orientation) to tilted and eventually to parallel (i.e., homeotropic orientation) with the increase of T_c . Recently, Hsiao et al. have used a set of PEO-*b*-PS single-crystal mats as a defect-free model system to understand the effects of confinement dimension and reduced tethering density on the crystal orientation.^{29–31} It was postulated that the transformation from homogeneous to homeotropic crystal orientation with increasing temperature occurred concomitantly with the transformation of the nucleation mechanism from homogeneous to heterogeneous nucleation.

In addition to PEO-containing systems, crystal orientation in a number of polyethylene (PE)-based C–A diblocks has been reported, including polyethylene-*b*-poly(ethylethylene) (PE-*b*-PEE),^{7,32} polyethylene-*b*-poly(ethylene-*alt*-propylene) (PE-*b*-PEP),^{7,33–35} and polyethylene-*b*-poly(vinylcyclohexane)

Received: October 29, 2010

Revised: January 19, 2011

Published: March 02, 2011

Table 1. Molecular Characteristics of the PE-*b*-PDLLA Used in the Present Study

weight fraction of PDLLA block ^a	volume fraction of PDLLA block ^b	\bar{M}_n (g·mol ⁻¹) ^c PDLLA block	\bar{M}_n (g·mol ⁻¹) ^c PE block	PE wt % 1,2 units	T_{ODT} (°C)	T_m^{PE} (°C)	T_g^{PDLLA} (°C)
0.54	0.47	32400	27700	1.15	7.0	>220	104

^a Experimental compositions as determined by ¹H NMR spectroscopy. ^b Calculated from the molecular weights and densities of PDLLA and PE blocks in the melt state. ^c Experimental \bar{M}_n estimated by ¹H NMR spectroscopy. ^d SEC versus polystyrene standards

(PE-*b*-PVCH).^{7,35} For these three symmetric diblocks, homogeneous crystal orientation with the *c*-axis of PE in the crystallites aligning perpendicular to \hat{n} was always observed, irrespective of whether the crystallization was subjected to a hard or soft confinement.

Crystal orientations in C-A diblock systems with other types of C blocks have also been addressed. Ho et al. have investigated the crystallization of the poly(L-lactide) (PLLA) block within the microphase-separated lamellar microdomain of poly(L-lactide)-block-poly(styrene) (PLLA-*b*-PS).²¹ This system was special in that the crystallization window of PLLA spanned from the temperature above T_g^{PS} to below T_g^{PS} , such that both soft and hard confinement to PLLA crystallization was accessible in a single copolymer. It was found that PLLA crystals always exhibited homeotropic orientation, irrespective of the confinement type.

Sun et al. have studied a series of lamellae-forming poly(ϵ -caprolactone)-block-poly(4-vinylpyridine) (PCL-*b*-P4VP),³⁶ where it was found that the domain thickness could control the crystal orientation and crystallization mechanism. The strong confinement induced not only a change of nucleation mechanism from heterogeneous to homogeneous nucleation but also a transformation in crystal orientation from homeotropic to homogeneous and even to random configuration.

In view of literature results, the crystal orientations in C-A diblock copolymers appear to be governed by several factors, including crystallization temperature, confinement size, and tethering density (or junction point cross section). It is worth noting that PE-containing diblocks seemed to behave anomalously, in that the crystals were reported to show homogeneous orientation while homeotropic orientation has not been observed so far. Considering that the crystallization of PE in previous studies was frequently induced by slowly cooling the sample to room temperature from the melt state, it remains unclear how the degree of undercooling (or T_c) would affect PE crystal orientation and whether homeotropic orientation is accessible. To resolve these issues, we undertake a systematic study to probe the PE crystal orientation in a lamellae-forming polyethylene-block-poly(D,L-lactide) (PE-*b*-PDLLA) (where PDLLA is racemic) over a broad range of T_c . Our previous work has shown that the crystallization of the PE block in the present C-A diblock was effectively confined within the lamellar microdomain, irrespective of whether T_c was above or below T_g^{PDLLA} (~ 55 °C).^{37–39} Consequently, the crystallization of the PE block can take place under either soft ($T_c > 55$ °C) or hard ($T_c < 55$ °C) confinement. In this work, we utilized 2D small-angle X-ray scattering (SAXS) and wide-angle X-ray diffraction (WAXD) to reveal the PE crystal orientation in the lamellar microdomains of the shear-oriented samples. It will be shown that the crystals displayed no preferred orientation at an intermediate to large nominal degree of undercooling ($\Delta T = T_m - T_c > \sim 65$ K, with T_m being the nominal melting point, ~ 104 °C). At higher T_c , PE crystals started to show homogeneous orientation, and such an orientation persisted even to very low ΔT (as low as 2 K). In light of this finding, we concluded that homogeneous orientation is an

intrinsic preferred orientation of PE crystals formed by the confined crystallization of PE-based block copolymers. Finally, we will organize and discuss the thermodynamic and kinetic factors that may govern the preferred crystal orientation for better understanding of the methodology for directional control of the crystalline nanostructures of block copolymers. We postulate that the competition between nucleation and crystal growth kinetics dictates the orientation behavior.

EXPERIMENTAL SECTION

Material. The synthesis of PE-*b*-PDLLA used in this study has been described in a previous publication.⁴⁰ Briefly, 1,3-butadiene was anionically polymerized in cyclohexane using sec-butyllithium as the initiator and subsequently end-capped with ethylene oxide to give hydroxyl-terminated 1,4-polybutadiene containing ~93% of the 1,4-regioisomer. This polybutadiene was then hydrogenated to give hydroxyl-terminated polyethylene, which was utilized in combination with AlEt₃ as a macroinitiator in the ring-opening polymerization of D,L-lactide (PDLLA). Because the PE block was prepared by hydrogenation of a 1,4-polybutadiene block, it can be considered as a random copolymer of ethylene and a low content of butene (approximately 7 wt %). Table 1 lists the molecular weight, composition, and the thermal properties of the diblock copolymer.

Sample Preparation. The copolymer samples for the crystallization studies were prepared by solvent casting. The copolymer was dissolved in toluene at 60 °C, yielding a 5% (w/v) solution. The solvent was evaporated slowly at 70 °C followed by further drying under vacuum at 70 °C for 2 days to remove the residual solvent.

Large-Amplitude Oscillatory Shear (LAOS) Experiment. Large-amplitude oscillatory shear was performed to produce large-scale alignment of the microdomains in PE-*b*-PDLLA. The shear was carried out with a Linkam CSS 450 shear hot stage in the oscillatory mode with the shear frequency of 0.3 Hz and the strain amplitude of 70%. The samples with the size of 5.0 × 5.0 × 0.2 mm³ were subjected to LAOS for 2 h under a nitrogen atmosphere at 140 °C to achieve good alignment of the lamellar microdomains. The shearing geometry is schematically illustrated in Figure 1. The shear direction is denoted as \hat{x} and the gradient direction is along \hat{z} . It will be shown that the lamellar normal (\hat{n}) is along \hat{z} .

Crystallization Treatment. The samples after shearing were further treated at prescribed crystallization temperatures. For $-50 \leq T_c \leq 102$ °C, the shear-oriented sample was first annealed at 170 °C in one Linkam HFS 91 hot stage for 15 min to erase the residual stresses and thermal histories. After 15 min, the sample was promptly transferred from the Linkam hot stage into the DSC sample chamber, which was pre-equilibrated at the prescribed T_c . The accuracy of sample temperature control was ±0.5 °C. All of the samples were kept at the T_c for a sufficiently long time in order to crystallize to saturation before SAXS/WAXD measurement. Longer crystallization time was employed at higher crystallization temperature. The PE crystallinities

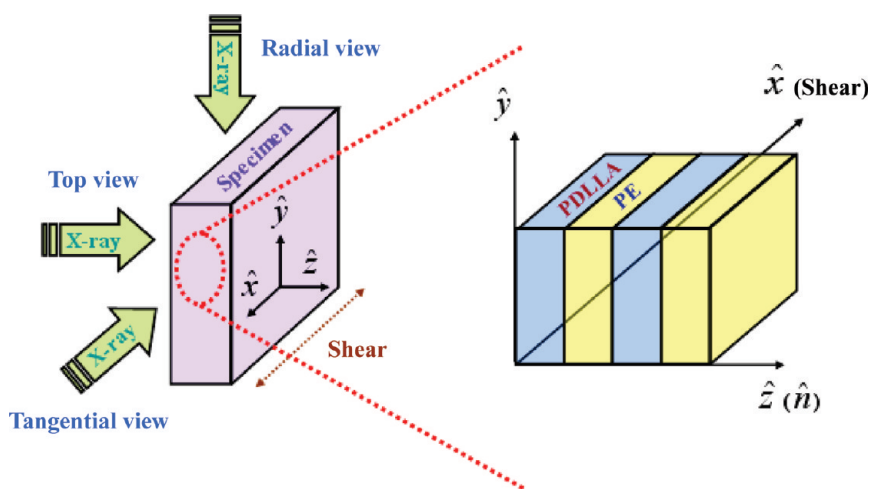


Figure 1. Schematic illustrations of the geometry of the shear-oriented PE-*b*-PDLLA specimen, indicating different incident directions of the X-ray for obtaining the 2-D scattering patterns in tangential view (the X-ray beam is traveling along \hat{x}), radial view (the X-ray is along \hat{y}), and top view (the X-ray is along \hat{z}). The illustration on the right shows the alignment of the lamellar microdomains attained after the shear treatment.

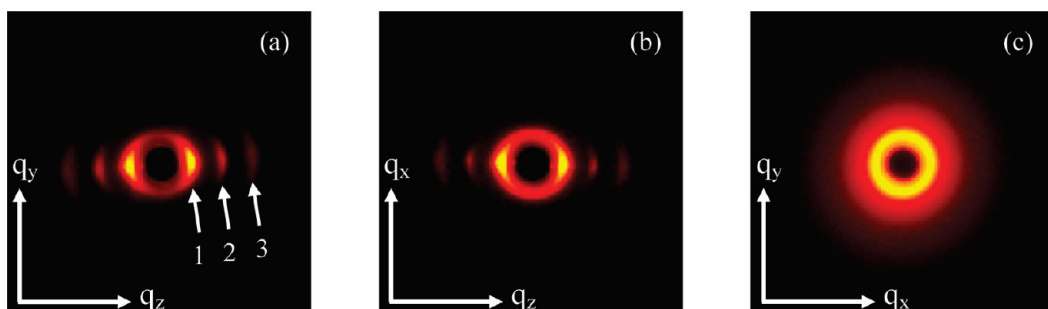


Figure 2. 2D SAXS patterns of shear-oriented PE-*b*-PDLLA after isothermal crystallization at $T_c = 97$ °C. (a) Tangential-view pattern; (b) radial-view pattern; (c) top-view pattern.

attained for all samples were around 0.40–0.45, as measured by the differential scanning calorimeter (DSC).

X-ray Scattering Experiments. SAXS experiments were performed at station BL23A1 at the National Synchrotron Radiation Research Center (NSRRC) located at Hsin-Chu, Taiwan.⁴¹ The energy of the X-ray source and the sample-to-detector distance were 8 keV ($\lambda = 0.155$ nm) and 2259 mm, respectively. The tangential-, radial-, and top-view SAXS patterns of the films were collected by having the incident X-ray traveling along \hat{x} , \hat{y} , and \hat{z} , respectively (see Figure 1). A two-dimensional Mar CCD detector with 512×512 pixel resolution was used to record the scattering pattern.

The WAXD measurements were performed at station BL17A1 at the NSRRC using an imaging plate as the detector. The X-ray beam with the wavelength of 1.334 Å was collimated into the beam size of 0.5 mm high and 3 mm wide by two slits separated by 1.1 mm. With a sample-to-detector distance of 212 mm, the diffraction patterns in tangential, radial, and top view were collected over the q range of 1–33 nm⁻¹.

RESULTS AND DISCUSSION

For the crystallization experiment, the shear-oriented samples of PE-*b*-PDLLA were first annealed at 170 °C for 15 min to erase the previous crystallization history followed by cooling to the desired T_c for crystallization. Figure 2 shows the representative 2D SAXS patterns of the sample having been crystallized at

97 °C. The scattering patterns obtained from tangential (Figure 2a) and radial view (Figure 2b) were practically identical, showing multiple reflections at the equator with the position ratio of 1:2:3, which indicated the presence of lamellar morphology with the interlamellar distance of 86 nm. The scattering patterns and the value of the interlamellar distance were essentially identical to those found in the melt state,³⁹ signaling that the melt morphology was effectively preserved upon PE crystallization. In other words, the crystallization was confined within the lamellar microdomains established in the melt state, although T_c was higher than T_g^{PDLLA} . The lamellar domains in the sheared sample were macroscopically aligned with the lamellar normal directed along \hat{z} (i.e., the gradient direction), as schematically illustrated in Figure 1. Similar SAXS patterns to those shown in Figure 2 were observed for other T_c 's (ranging from –50 to 102 °C; see Figure S1 in Supporting Information).

Figure 3 displays the corresponding 2D WAXD patterns of PE-*b*-PDLLA having been crystallized at 97 °C. The diffraction patterns of the samples crystallized at $45 \leq T_c \leq 102$ °C were indeed similar (see Figure S1 in Supporting Information). The anisotropic diffraction patterns associated with PE crystals obtained from tangential (along \hat{x}) and radial (along \hat{y}) view were essentially identical, whereas that obtained from the top view (along \hat{z}) showed isotropic rings. This means that PE crystal orientation in the lamellar microdomains was identical when viewed along the \hat{x} and \hat{y} directions, but the orientation was

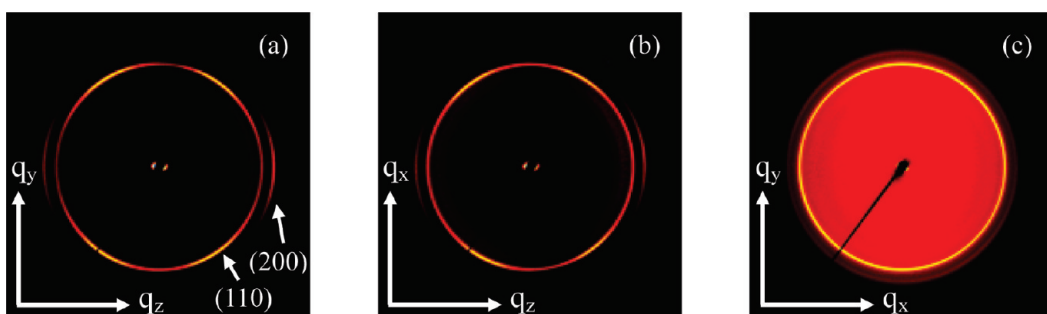


Figure 3. 2D WAXD patterns of shear-oriented PE-*b*-PDLLA after isothermal crystallization at $T_c = 97^\circ\text{C}$. (a) Tangential-view pattern; (b) radial-view pattern; (c) top-view pattern.

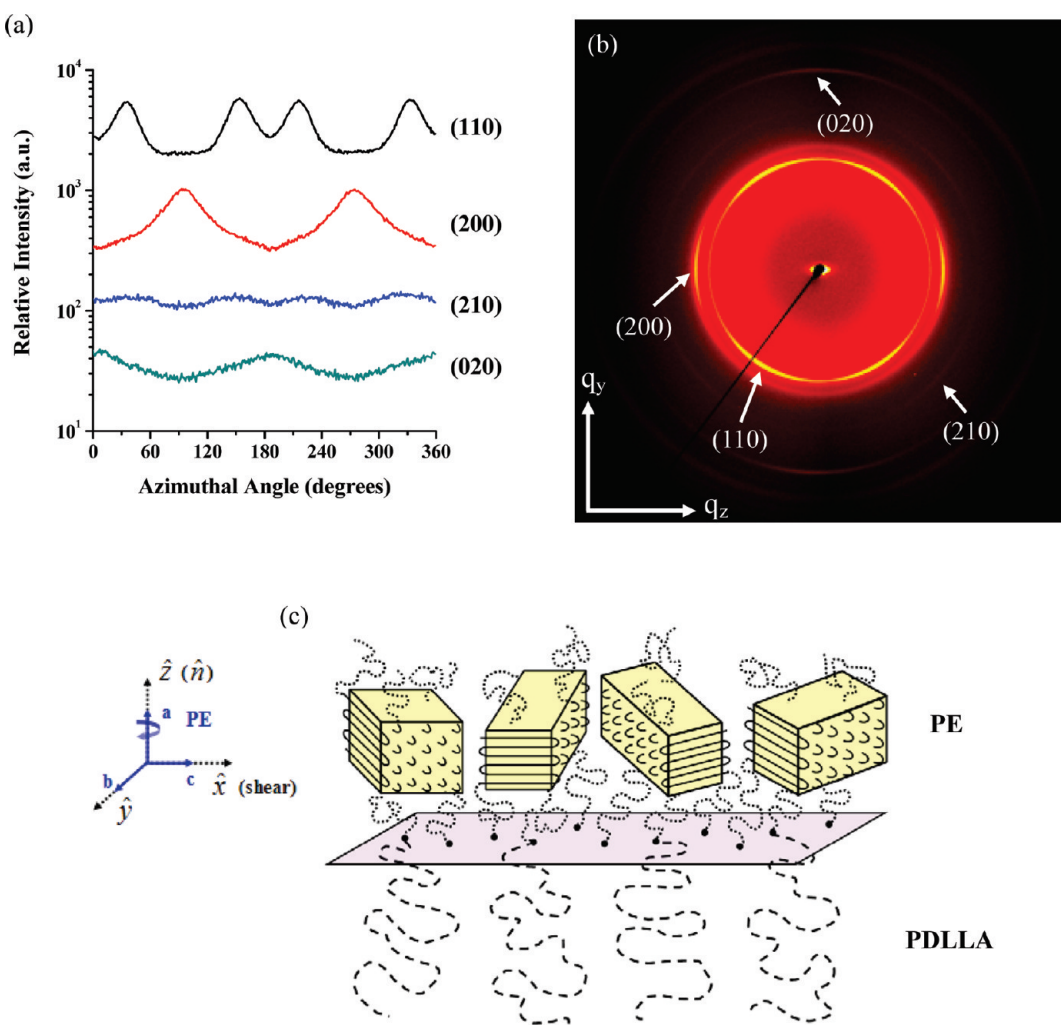


Figure 4. (a) The azimuthal scans of (110), (200), (210), and (020) diffractions of PE crystal; (b) 2D WAXD pattern showing that (200) and (020) diffractions are orthogonal to each other; (c) schematic presentation of homogeneous crystal orientation with the PE crystalline stems aligning parallel to the lamellar interface.

random when viewed along \hat{z} . The (110) and (200) diffractions at $q = 15.2$ and 16.8 nm^{-1} were observed in the quadrants and the equator, respectively, in the anisotropic patterns. From the azimuthal scans (obtained by scanning the intensity of a specific diffraction around the azimuthal angle starting from the vertical direction of the pattern) of (110), (200), (210), and (020) diffractions shown in Figure 4a, the angles between the (110) and (200) and between the (210) and (200) planes were found to be

56.3 and 52.6° , respectively, which closely agreed with those reported previously from the fiber pattern.⁴² Because (200) diffractions in both tangential and radial view of the WAXD patterns were located at the same direction (i.e., at the equator) as the lamellar scattering peaks in the corresponding SAXS patterns and (200) and (020) crystal diffractions were orthogonal to each other (Figure 4b), the *c*-axis or the direction of the crystalline stem was deduced to align perpendicular to the

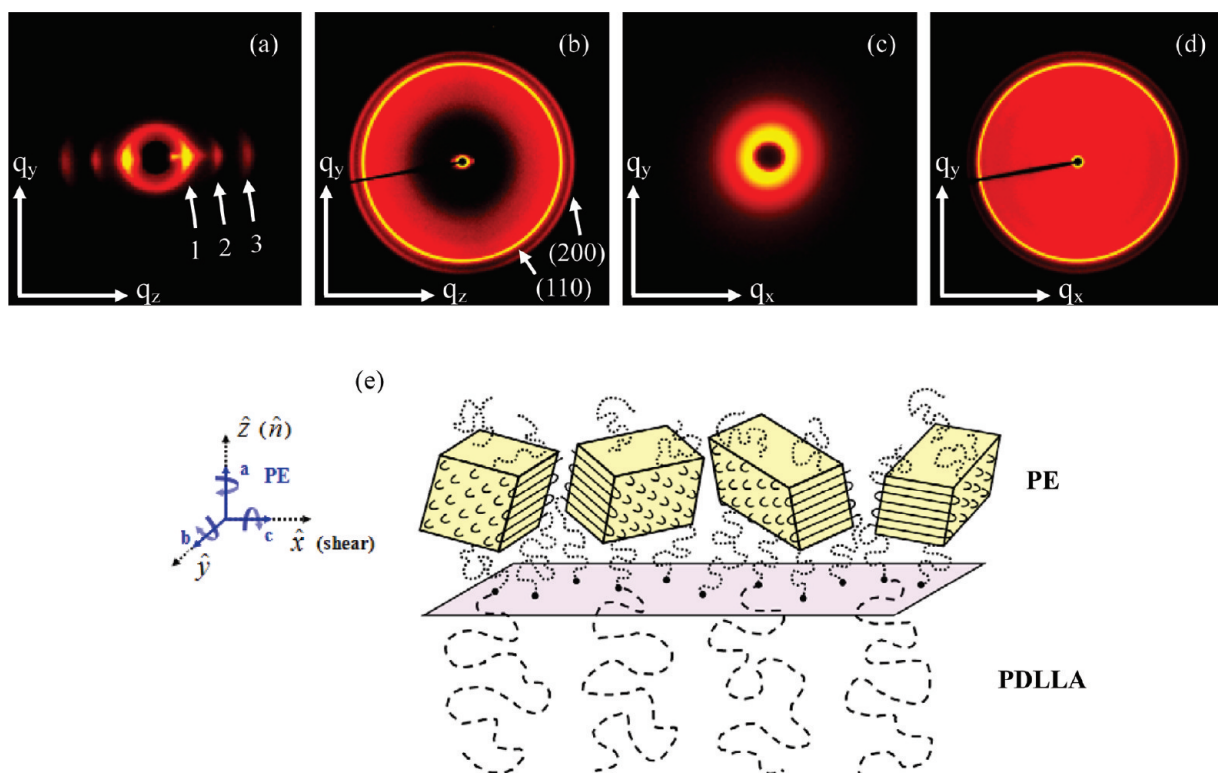


Figure 5. 2D SAXS/WAXD patterns of shear-oriented PE-*b*-PDLLA after crystallization at $T_c = 40$ °C. (a) Tangential-view SAXS pattern; (b) tangential-view WAXD pattern; (c) top-view SAXS pattern; (d) top-view WAXD pattern; (e) schematic presentation of random orientation of PE crystals in the lamellar microdomain.

lamellar normal (or parallel to the lamellar interface). However, when looking along \hat{z} (or the lamellar normal), the a -axis of the crystals did not show preferred orientation, as indicated by the isotropic WAXD pattern obtained from the top view.

On the basis of the X-ray scattering patterns, the organization of PE crystals in the lamellar microdomains over $45 \leq T_c \leq 102$ °C is schematically illustrated in Figure 4c. The crystals were found to exhibit homogeneous orientation with the crystalline stems aligning parallel to the lamellar interface. Such a crystal orientation was consistent with the previous findings for other PE-containing crystalline–amorphous diblock copolymers. It is important to note that homogeneous orientation was still dominant even at $T_c = 102$ °C, which was only 2 K below the nominal melting point of PE block.

Figure 5 shows the representative 2D SAXS and WAXD patterns of shear-oriented PE-*b*-PDLLA having been crystallized at $T_c = 40$ °C $< T_g^{\text{PDLLA}}$, where the crystallization of PE block occurred under hard confinement. Similar scattering patterns were observed for isothermal crystallization at the lower T_c 's or for crystallization induced by directly quenching the sample into liquid nitrogen from the melt (see Figure S1 in Supporting Information). Because the tangential- and radial-view patterns were identical, only the former are displayed in Figure 5. Analogous to that found in Figure 2, the SAXS pattern in tangential view displays a series of arcs situated at the equator, showing the presence of macroscopically aligned lamellar microdomains established by the microphase separation in the melt state. However, the corresponding WAXD patterns display isotropic rings, signaling that the PE crystals were randomly oriented in the microdomains, as schematically illustrated in Figure 5e.

The transformation of crystal orientation at 40–45 °C can be further demonstrated by the T_c dependence of the Herman's orientation function (f) evaluated using the intensity distribution of both (110) and (200) diffractions along the azimuthal angle (ϕ) of the 2-D scattering pattern.⁴³ For f calculated using (200) diffraction, the tangential-view patterns were analyzed, and the \hat{y} axis was taken as the reference direction; f has a value of 1.0 when the normal of the diffraction plane is parallel to the reference direction (i.e., $\phi = 0^\circ$), a value of -0.5 means a perpendicular orientation of the diffraction plane normal to the reference direction (i.e., $\phi = 90^\circ$), and a value of 0 signals random crystal orientation. The orientation function associated with the (110) plane was calculated according to the procedure reported previously.⁴⁴ The dependences of the values of f on T_c are displayed in Figure 6. It is seen that the orientation functions associated with both (110) and (200) diffractions change slightly with decreasing T_c at $45 \leq T_c \leq 60$ °C, but it decreases and increases abruptly across 40–45 °C, respectively. The T_c dependences of f reveals that the crystal orientation changes abruptly from homogeneous to random orientation at 40–45 °C.

The 2D SAXS/WAXD patterns of the shear-oriented PE-*b*-PDLLA crystallized over a broad range of T_c ($-50 \leq T_c \leq 102$ °C) revealed that the orientation of PE crystals transformed from random orientation (at relatively large undercooling) to homogeneous orientation (at lower undercooling). However, in contrast to PEO-*b*-PS and other C–A diblocks where homeotropic orientation was predominantly observed at moderate to low undercooling, such an orientation was not identified for the present system even at very low undercooling.

On basis of the present work (i.e., PE-*b*-PDLLA system) and the results of other PE-based C–A diblocks having been

reported previously (i.e., PE-*b*-PEE, PE-*b*-PEP, PE-*b*-PVCH, etc.)^{7,32–35} we concluded that when there was a preferred orientation, PE crystals formed in the lamellar microdomains always tended to show homogeneous orientation. It should be indicated that the PE blocks in nearly all of these copolymers (including the present system) were prepared by hydrogenation of 1,4-polybutadiene precursors which may contain about 10% vinyl repeat unit; in this case, the PE blocks inevitably contained $\sim 2\text{--}3$ ethyl branch defects per 100 carbon atoms. It may thus be speculated that the accommodation of the short branches excluded out of the crystalline stems in the crystals could be responsible for the atypical homogeneous crystal orientation. This possibility can however be precluded by considering the work of Cohen et al., who used a PE-*b*-PS with an essentially defect-free PE block for studying the crystal orientation.⁴⁵ According to the pole figure analysis, it was found that the *a*-axis of the PE unit cell oriented normal to the lamellar interface, while the *b*- and *c*-axes (and thus the crystalline stem) arranged randomly, which were similar to the results found earlier using the branch-containing PE block.³² Recently, Myers et al. have developed a synthetic route to prepare a set of defect-free PE-*b*-PVCH by hydrogenation of polycyclopentene (PCP) and PS blocks in PCP-*b*-PS.⁴⁶ They further reported the morphology and crystal orientation within various types of PE microdomains, covering spherical, cylindrical, and lamellar structures.⁴⁷ In the

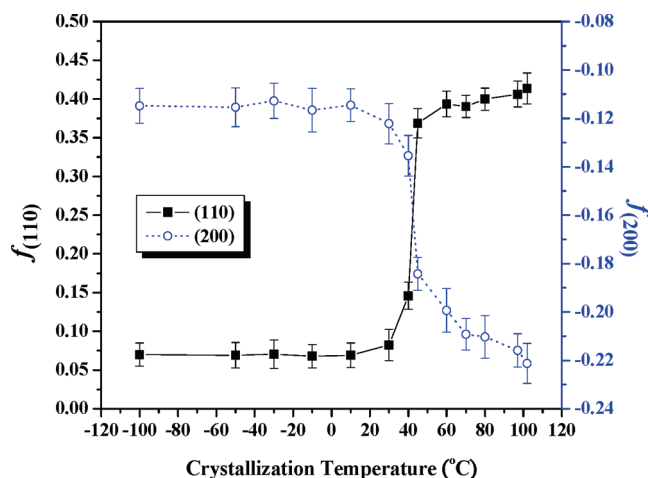


Figure 6. Herman's orientation function (f) calculated using the azimuthal distributions of the intensities of (110) (closed square) and (200) (open circle) diffractions as a function of crystallization temperatures.

case of the lamellar domain, homogeneous orientation was again observed. Therefore, it can be concluded that the commonly observed homogeneous orientation of PE crystals in microphase-separated lamellar microdomains is not related to the existence of short branch defects.

In order to reveal the crystal orientation, samples with large-scale orientation of microdomains were normally prepared by shearing in the melt state. The shearing allowed the lamellar interface to align preferentially along the shear direction (see Figure 1), and hence, the PE block chains might also be stretched toward the shear direction. If the stretching of PE block is not completely relaxed before crystallization, the orientational memory may cause the crystalline stem to align parallel to the lamellar interface so as to give rise to the homogeneous orientation. To test if this memory effect was responsible for the homogeneous crystal orientation, we examined the crystal orientation in the samples having been subjected to prolonged melt annealing to relax the possible chain orientation. Figure 7a–c shows the 2D WAXD patterns of PE-*b*-PDLLA, having been annealed at 170 °C for 5 h under a nitrogen atmosphere, followed by cooling to 97 °C for crystallization. Again, the anisotropic diffraction patterns revealed homogeneous crystal orientation, and the degree of orientation was not poorer. This finding verified that the homogeneous orientation should not stem from the memory of the possible chain orientation in the melt.

On the basis of the above discussion, we concluded that homogeneous orientation is an intrinsically favored arrangement of PE crystals in the lamellar microdomains. A previous coarse-grained simulation study by Hu et al.⁴⁸ revealed that in the melt state, the segments of the block chains near the lamellar interface tend to align normal to the interface. Such a preferred segmental orientation would lead to homeotropic crystal orientation once the nucleation starts near the interfacial region. This simulation result thus suggests that homeotropic orientation is favored due to junction point constraint. The homogeneous orientation observed predominantly among PE-based diblocks is not consistent with this prediction.

A recent study of the change of PEO crystal orientation with respect to T_c by Hsiao and Cheng et al. postulated that the transformation from homogeneous to homeotropic orientation was related to the change of nucleation mechanism from homogeneous nucleation to heterogeneous nucleation.^{30,31} Because homogeneous nucleation normally occurs at very large undercooling, where the nuclei explode in the system, leading to very high nucleation density, this implies that homogeneous crystal orientation may be related to high nucleation density in the crystallization process.

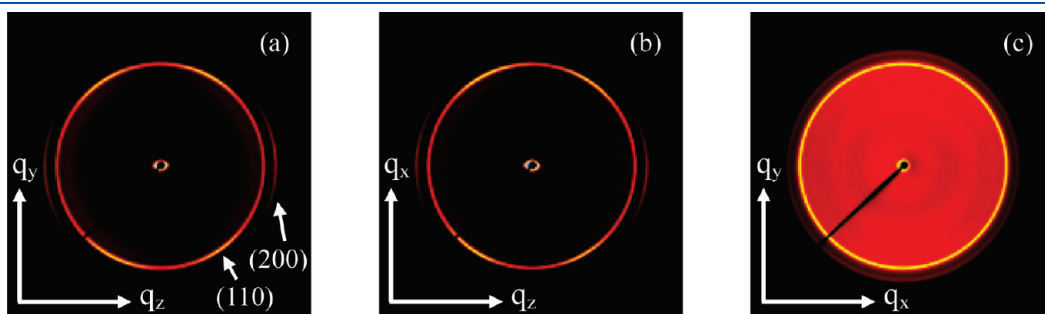


Figure 7. 2D WAXD patterns of shear-oriented PE-*b*-PDLLA after isothermal crystallization at 97 °C. Prior to the crystallization, the sample was annealed at 170 °C for 5 h to release the possible memory of PE chain stretching. (a) Tangential-view pattern; (b) radial-view pattern; (c) top-view pattern.

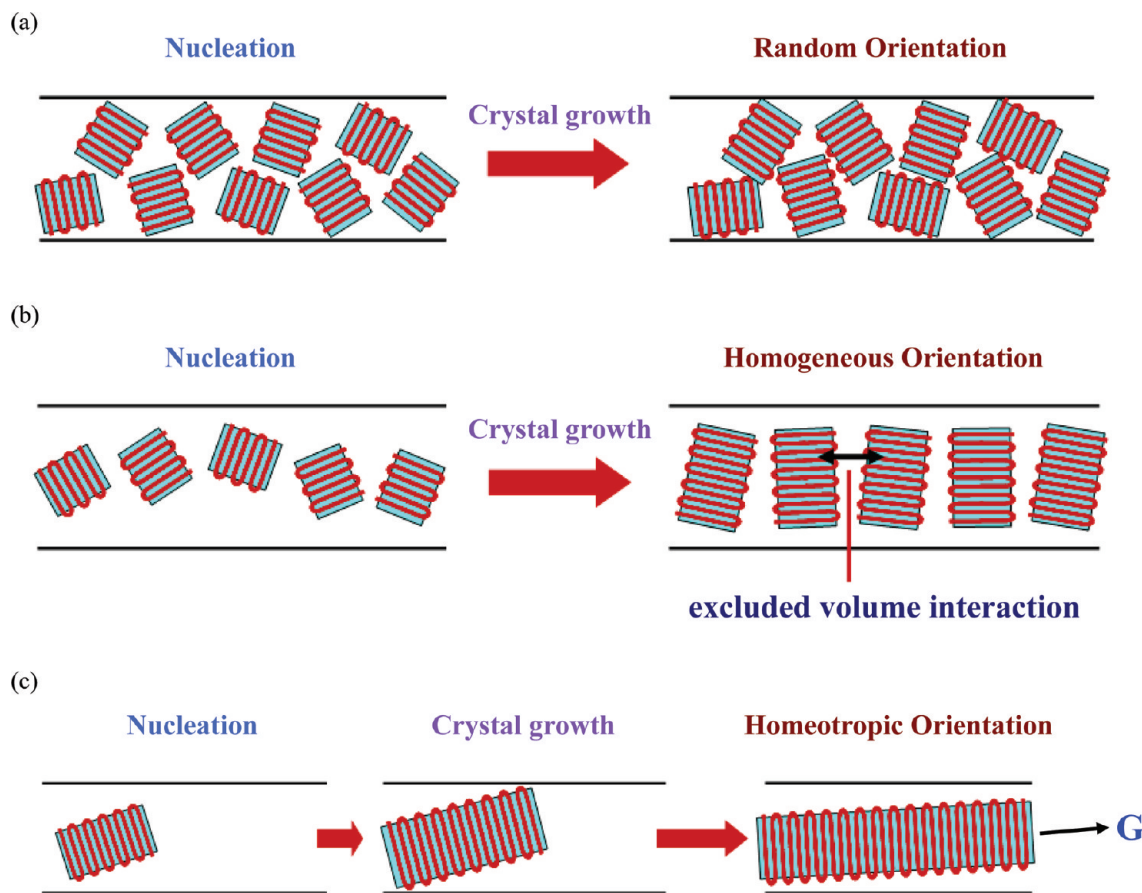


Figure 8. Schematic illustration showing the control of crystal orientation by the competition between nucleation and crystal growth kinetics. (a) At very large undercooling, a large number of nuclei exploded in the microdomain almost simultaneously. The domain was quickly filled with randomly oriented nuclei, and the jamming of these crystallites frustrated the crystal growth, thereby leading to random orientation eventually. (b) At lower undercooling, the nucleation density was still quite high, but the crystal growth was operative in the domain. The growing lamellae-shaped crystallites experienced an excluded volume interaction to yield homogeneous orientation. (c) At low undercooling, where the nucleation density was small. The crystal would adjust its orientation to facilitate long-range growth and eventually adopted homeotropic orientation.

Here, we evoke a kinetic reasoning which postulates that the crystal orientation is governed by the competition between nucleation rate and crystal growth kinetics. When a given nucleus appears within the lamellar microdomain, it should not feel the confinement effect because its size is much smaller than the lamellar thickness (cf. the critical thickness of the PE nucleus at $\Delta T \approx 70$ K is ca. 4 nm); therefore, most nuclei developed in the domain are most likely randomly oriented.¹⁴ At very large undercooling, where the nucleation is extremely rapid, a great number of nuclei explode in the microdomain almost simultaneously. The volume is then quickly filled with randomly oriented nuclei, and the jamming of these crystallites frustrates the crystal growth, leading eventually to crystals in random orientation (Figure 8a).

At the lower undercooling where the nucleation density is not exceedingly high (but is still quite high), the crystal growth becomes operative within the microdomain. The growing crystals, which are disk or lamellae in shape, may experience an excluded volume interaction when two of them are sufficiently close. This is reminiscent of the interaction between discotic liquid crystalline molecules that gives rise to a regular stacking of the molecules to form a columnar mesophase. Once this type of interaction is significant, the crystals should stack along the lamellar interface, as schematically illustrated in Figure 8b to generate a homogeneous crystal orientation.

The nucleation rate becomes slow when the degree of undercooling is small. Hence, the crystal grown from a given nucleus may not feel the interference from another crystal before the growth front impinges the lamellar interface. Under this condition, the crystal would adjust its orientation to facilitate long-range growth and eventually adopt homeotropic orientation (Figure 8c).

On the basis of our kinetic reasoning, the preferred homogeneous orientation of PE-based diblocks may thus be attributed to the good nucleating power of PE block in the lamellar microdomain. It has been found that homogeneous nucleation of PE was able to take place at a relatively small critical degree of undercooling ($\Delta T_{cr} \approx 40$ K)^{20,22,49} in comparison to other semicrystalline polymers (e.g., $T_{cr} \approx 90$ K for PEO; $T_{cr} \approx 100$ K for PCL) in block copolymer systems.^{10,50} It is also well-known that, even in the bulk, polyethylene has an intrinsically high density of active nuclei (on the order of 10^9 nuclei/cm³, at least 3 orders of magnitude larger than PEO and PCL).^{20,51} All of the above suggest that PE indeed has an excellent nucleating power and that may lead to the persistence of homogeneous orientation in the diblock copolymers.

Finally, we would like to note that the T_c range (i.e., 40–45 °C) at which the transition from homogeneous to random orientation in the present PE-*b*-PDLLA occurred was in the

vicinity of the T_g of PDLLA, which implied that vitrification of the amorphous block may play a role to cause random crystal orientation. As the crystal growth should involve a relatively long-range transport of PE segments to the growth front, the growth of PE crystals may become highly frustrated due to the great constraint of the diffusion of junction points at the interface while PE is anchored to the glassy PDLLA microdomain. In this case, nucleation could dominate the crystallization more easily and consequently lead to random orientation of the crystals.

CONCLUSIONS

The orientation of PE crystals formed in the lamellar micro-domains of a crystalline–amorphous PE-*b*-PDLLA has been revealed over a broad range of T_c . The crystals formed at a relatively large nominal degree of undercooling ($\Delta T > \approx 65$ K) were randomly orientated. Homogeneous orientation with crystalline stems aligning parallel to the lamellar interface was observed at higher T_c , while homeotropic orientation was not found even at very low undercooling (as low as 2 K). We postulated that the crystal orientation was governed by the competition between nucleation rate and crystal growth kinetics. At very large undercooling, the very high number density of the randomly oriented nuclei frustrated the crystal growth in the microdomain and hence led to random crystal orientation. Increasing T_c reduced the nucleation density, and the excluded volume interaction between lamellae-shaped growing crystallites resulted in homogeneous orientation. At small undercooling, the nucleation density was so low that the crystal growth could proceed over a rather long-range (\gg the lamellar domain thickness). In this case, the homeotropic orientation which favors long-range crystal growth should be observed. On basis of this kinetics reasoning, the homogeneous crystal orientation found prevalently among PE-based diblock copolymers was attributed to the excellent nucleating power of PE block in the lamellar microdomain.

ASSOCIATED CONTENT

S Supporting Information. The 2D SAXS/WAXD patterns of shear-oriented PE-*b*-PDLLA after crystallizations at 102, 80, 70, 60, 45, 30, 10, -10, -30, and -50 °C or directly quenching into liquid nitrogen from the melt. This material is available free of charge via the Internet at <http://pubs.acs.org>.

AUTHOR INFORMATION

Corresponding Author

*E-mail: hlchen@che.nthu.edu.tw.

ACKNOWLEDGMENT

We acknowledge Professor Marc A. Hillmyer for providing the block copolymers used in this study. We thank Kelly Anderson for the synthesis of the block copolymers and Marc Rodwogin for his help with an initial morphology determination by SAXS. We also thank to the National Synchrotron Radiation Center, Hsin-Chu, Taiwan, for support in the X-ray scattering experiments. Finally, we acknowledge the support from the National Science Council under Grant NSC 99-2221-E-007-008.

REFERENCES

- (1) Hamley, I. W. *The Physics of Block Copolymers*; Oxford University Press: New York, 1998; Chapter 5.
- (2) Müller, A. J.; Balsamo, V.; Arnal, M. L. *Adv. Polym. Sci.* **2005**, *190*, 1–63.
- (3) Müller, A. J.; Balsamo, V.; Arnal, M. L. In *Progress in Understanding of Polymer Crystallization*; Reiter, G., Strobl, G., Eds.; Springer: Berlin, Germany, 2007; Vol. 714, pp 229–259.
- (4) Ryan, A. J.; Hamley, I. W.; Bras, W.; Bates, F. S. *Macromolecules* **1995**, *28*, 3860–3868.
- (5) Ryan, A. J.; Fairclough, J. P. A.; Hamley, I. W.; Mai, S. M.; Booth, C. *Macromolecules* **1997**, *30*, 1723–1727.
- (6) Quiram, D. J.; Register, R. A.; Marchand, G. R. *Macromolecules* **1997**, *30*, 4551–4558.
- (7) Hamley, I. W.; Fairclough, J. P. A.; Terrill, N. J.; Ryan, A. J.; Lipic, P. M.; Bates, F. S.; Towns-Andrews, E. *Macromolecules* **1996**, *29*, 8835–8843.
- (8) Nojima, S.; Kato, K.; Yamamoto, S.; Ashida, T. *Macromolecules* **1992**, *25*, 2237–2242.
- (9) Rangarajan, P.; Register, R. A.; Fetter, L. J.; Bras, W.; Naylor, S.; Ryan, A. J. *Macromolecules* **1995**, *28*, 4932–4938.
- (10) Chen, H. L.; Wu, J. C.; Lin, T. L.; Lin, J. S. *Macromolecules* **2001**, *34*, 6936–6944.
- (11) Chen, H. L.; Hsiao, S. C.; Lin, T. L.; Yamauchi, K.; Hasegawa, H.; Hashimoto, T. *Macromolecules* **2001**, *34*, 671–674.
- (12) Lee, W.; Chen, H. L.; Lin, T. L. *J. Polym. Sci., Part B: Polym. Phys.* **2002**, *40*, 519–529.
- (13) Shiomi, T.; Takeshita, H.; Kawaguchi, H.; Nagai, M.; Takenaka, K.; Miya, M. *Macromolecules* **2002**, *35*, 8056–8065.
- (14) Zhu, L.; Cheng, S. Z. D.; Calhoun, B. H.; Ge, Q.; Quirk, R. P.; Thomas, E. L.; Hsiao, B. S.; Yeh, F.; Lotz, B. *J. Am. Chem. Soc.* **2000**, *122*, 5957–5967.
- (15) Takeshita, H.; Ishii, N.; Araki, C.; Miya, M.; Takenaka, K.; Shiomi, T. *J. Polym. Sci., Part B: Polym. Phys.* **2004**, *42*, 4199–4206.
- (16) Weimann, P. A.; Hajduk, P. A.; Hajduk, D. A.; Chu, C.; Chaffin, K. A.; Brodin, J. C.; Bates, F. S. *J. Polym. Sci., Part B: Polym. Phys.* **1999**, *37*, 2053–2068.
- (17) Arnal, M. L.; Balsamo, V.; Lopez-Carrasco, F.; Contreras, J.; Carrillo, M.; Schmalz, H.; Abetz, V.; Laredo, E.; Müller, A. J. *Macromolecules* **2001**, *34*, 7973–7982.
- (18) Zhu, L.; Cheng, S. Z. D.; Calhoun, B. H.; Ge, Q.; Quirk, R. P.; Thomas, E. L.; Hsiao, B. S.; Yeh, F.; Lotz, B. *Polymer* **2001**, *42*, 9121–9131.
- (19) Loo, Y. L.; Register, R. A.; Ryan, A. J. *Macromolecules* **2002**, *35*, 2365–2374.
- (20) Müller, A. J.; Balsamo, V.; Arnal, M. L.; Jakob, T.; Schmalz, H.; Abetz, V. *Macromolecules* **2002**, *35*, 3048–3058.
- (21) Ho, R. M.; Lin, F. H.; Tsai, C. C.; Lin, C. C.; Ko, B. T.; Hsiao, B. S.; Sics, I. *Macromolecules* **2004**, *37*, 5985–5994.
- (22) Loo, Y. L.; Register, R. A.; Ryan, A. J. *Phys. Rev. Lett.* **2000**, *84*, 4120–4123.
- (23) Loo, Y. L.; Register, R. A.; Adamson, D. H. *Macromolecules* **2000**, *33*, 8361–8366.
- (24) Loo, Y. L.; Register, R. A.; Ryan, A. J.; Dee, G. T. *Macromolecules* **2001**, *34*, 8968–8977.
- (25) Lotz, B.; Kovacs, A. J. *Kolloid Z. Z. Polym.* **1966**, *209*, 97–114.
- (26) Kovacs, A. J.; Lotz, B.; Keller, A. J. *Macromol. Sci. Phys.* **1969**, *B3*, 385–425.
- (27) Hirata, E.; Ijitsu, T.; Soen, T.; Hashimoto, T.; Kawai, H. *Polymer* **1975**, *16*, 249–260.
- (28) Yang, Y. W.; Tanodekaew, S.; Mai, S. M.; Booth, C.; Ryan, A. J.; Bras, W.; Viras, K. *Macromolecules* **1995**, *28*, 6029–6041.
- (29) Hsiao, M. S.; Chen, W. Y.; Zheng, J. X.; Van Horn, R. M.; Quirk, R. P.; Ivanov, D. A.; Thomas, E. L.; Lotz, B.; Cheng, S. Z. D. *Macromolecules* **2008**, *41*, 4794–4801.
- (30) Hsiao, M. S.; Zheng, J. X.; Leng, S.; Van Horn, R. M.; Quirk, R. P.; Thomas, E. L.; Chen, H. L.; Hsiao, B. S.; Rong, L.; Lotz, B.; Cheng, S. Z. D. *Macromolecules* **2008**, *41*, 8114–8123.
- (31) Hsiao, M. S.; Zheng, J. X.; Van Horn, R. M.; Quirk, R. P.; Thomas, E. L.; Chen, H. L.; Lotz, B.; Cheng, S. Z. D. *Macromolecules* **2009**, *42*, 8343–8352.

- (32) Douzinas, K. C.; Cohen, R. E. *Macromolecules* **1992**, *25*, 5030–5035.
- (33) Séguéla, R.; Prud'homme, J. *Polymer* **1989**, *30*, 1446–1455.
- (34) Kofinas, P.; Cohen, R. E. *Macromolecules* **1994**, *27*, 3002–3008.
- (35) Hamley, I. W.; Fairclough, J. P. A.; Ryan, A. J.; Bates, F. S.; Towns-Andrews, E. *Polymer* **1996**, *37*, 4425–4429.
- (36) Sun, Y. S.; Chung, T. M.; Li, Y. J.; Ho, R. M.; Ko, B. T.; Jeng, U. S.; Lotz, B. *Macromolecules* **2006**, *39*, 5782–5788.
- (37) Müller, A. J.; Castillo, R. V.; Hillmyer, M. A. *Macromol. Symp.* **2006**, *242*, 174–181.
- (38) Müller, A. J.; Lorenzo, A. T.; Castillo, R. V.; Arnal, M. L.; Boschetti-De-Fierro, A.; Abetz, V. *Macromol. Symp.* **2006**, *245*, 154–160.
- (39) Castillo, R. V.; Müller, A. J.; Lin, M. C.; Chen, H. L.; Jeng, U. S.; Hillmyer, M. A. *Macromolecules* **2008**, *41*, 6154–6164.
- (40) Anderson, K. S.; Hillmyer, M. A. *Polymer* **2004**, *45*, 8809–8823.
- (41) Jeng, U. S.; Su, C. H.; Su, C. J.; Liao, K. F.; Chuang, W. T.; Lai, Y. H.; Chang, J. W.; Chen, Y. J.; Huang, Y. S.; Lee, M. T.; Yu, K. L.; Lin, J. M.; Liu, D. G.; Chang, C. F.; Liu, C. Y.; Chang, C. H.; Liang, K. S. *J. Appl. Crystallogr.* **2010**, *43*, 110–121.
- (42) Zugenmaier, P.; Cantow, H. J. *Kolloid Z. Z. Polym.* **1969**, *230*, 229–236.
- (43) Alexander, L. E. *X-ray Diffraction in Polymer Science*; Wiley: New York, 1969.
- (44) Nojima, S.; Ohguma, Y.; Kadena, K.; Ishizone, T.; Iwasaki, Y.; Yamaguchi, K. *Macromolecules* **2010**, *43*, 3916–3923.
- (45) Cohen, R. E.; Bellare, A.; Drzewinski, M. A. *Macromolecules* **1994**, *27*, 2321–2323.
- (46) Myers, S. B.; Register, R. A. *Macromolecules* **2008**, *41*, 5283–5288.
- (47) Myers, S. B.; Register, R. A. *Macromolecules* **2010**, *43*, 393–401.
- (48) Hu, W. B.; Frenkel, D. *Faraday Discuss.* **2005**, *128*, 253–260.
- (49) Quiram, D. J.; Register, R. A.; Marchand, G. R.; Adamson, D. H. *Macromolecules* **1998**, *31*, 4891–4898.
- (50) Hsu, J. Y.; Hsieh, I. F.; Nandan, B.; Chiu, F. C.; Chen, J. H.; Jeng, U. S.; Chen, H. L. *Macromolecules* **2007**, *40*, 5014–5022.
- (51) Arnal, M. L.; Matos, M. E.; Morales, R. A.; Santana, O. O.; Müller, A. J. *Macromol. Chem. Phys.* **1998**, *199*, 2275–2298.